DOI: 10.1002/ejic.200900090

Supramolecular Architectures and Magnetic Properties of Self-Assembled Windmill-Like Dinuclear Copper(II) Complexes with Purine Ligands

Javier Cepeda,[a] Oscar Castillo,*[a] Juan P. García-Terán,[a] Antonio Luque,*[a] Sonia Pérez-Yáñez,[a] and Pascual Román[a]

Keywords: Nitrogen heterocycles / Copper / Magnetic properties / Density functional calculations / Supramolecular chemistry

Three new Cu^{II} compounds, $[Cu_2(\mu\text{-ade})_4(H_2O)_2]\cdot(bpa)\cdot 8H_2O$ (**1**), $[Cu_2(\mu\text{-Hade})_4(H_2O)_2](NO_3)_4\cdot 2[Cu(pic)_2(H_2O)]\cdot 6H_2O$ (**2**) and $[Cu_2(\mu\text{-6Clpur})_4(H_2O)_2]\cdot\sim 6H_2O$ (**3**) [in which ade = adeninate anion, Hade = 7*H*-adenine, 6Clpur = 6-chloropurinate anion, bpa = 1,2-bis(4-pyridyl)ethane, pic = 2-pyridinecarboxylate anion], are reported. Their crystal structures consist of dinuclear copper(II) units, in which four ligands arranged in a windmill-like fashion bridge the metal ions through a nonlinear NCN group. Supramolecular crystal building of compound **1** is essentially maintained by an extensive network of hydrogen-bonding interactions that involves direct contacts between the nucleobases. In contrast, in compound **2** there is no evidence for direct interactions between the nucleobases, but the hydrogen bonds among the nucleobases and nitrate counteranions are especially relevant. Compound **3** is mainly built up from T-shaped noncovalent Cl···N interactions and hydrogen-bonding interactions involving the crystallization solvent molecules. Magnetic susceptibility measurements indicate the presence of strong intradimeric antiferromagnetic interactions with large singlet–triplet splittings of –222 (for **1**), –288 (for **2**) and –255 (for **3**) cm^{-1}. DFT calculations were carried out to evaluate the dependence of the magnetic coupling value as a function of some key structural parameters: the Cu–N basal plane distance, the axial Cu–Ow distance and the Cu···Cu distance. DFT calculations also revealed that the nature of the bridging ligand is a crucial factor. In this way, the strength to transmit the magnetic interaction of the different bridging ligands is explained on the basis of the number of electron lone pairs.

Introduction

The chemistry of dinuclear copper(II) compounds has been extensively studied over many decades in order to understand the spin-exchange interaction that allows us to establish magnetostructural relationships.[1] In fact, the phenomenon of magnetic exchange was first reported for the dinuclear $[Cu_2(\mu\text{-}CH_3COO)_4(H_2O)_2]$ complex.[2] In later years, X-ray and magnetic investigations were extended to other related $[Cu_2(L)_4]$ systems (L = purine derivatives)[3–7] containing biologically relevant entities. These kinds of entities, characterized by their striking windmill arrangement, are of high interest because of their structural and magnetic properties. The choice of the purine ligands as bridging ligand is due to their great ability to build dinuclear complexes by means of the μ-κ*N3*:κ*N9* predominant bridging mode.

In contrast, dinuclear complexes made up of square-planar transition-metal ions (M) with four heterocyclic ligands (L) carrying additional functionalities are potential building blocks for supramolecular architectures involving hydrogen-bond formation, cation binding or anion binding.[8] In particular, hydrogen-bonding interactions have been established as a reliable force for organic crystal engineering,[9] but these interactions have only been introduced lately as a tool for the supramolecular assembly of coordination complexes by Mingos and co-workers.[10] Early examples of supramolecular assemblies have been provided for "host–guest" compounds in which a larger "host" molecule includes a smaller "guest" molecule within a cavity in its structure.[11] Adenine is known to establish various molecular recognition patterns with molecules that are compatible with its hydrogen-bonding scheme.[12] In this way, the inclusion of additional species within the structure of adenine-containing dinuclear entities provides a better understanding of the preponderance of these hydrogen-bonding patterns.

Compounds with the $[Cu_2(L)_4]$ core have the same type of molecular structure, in which the presence of nonlinear bridging NCN group provides an efficient pathway for magnetic coupling.[13] The interaction between the spins of both metal atoms through the ligand leads to splitting in two electronic states, giving rise to a singlet ($S = 0$) and a triplet ($S = 1$). The energetic difference between these states (J)

[a] Departamento de Química Inorgánica, Facultad de Ciencia y Tecnología, Universidad del País Vasco,
Apartado 644, 48080 Bilbao, Spain
Fax: +34-94601-3500
E-mail: oscar.castillo@ehu.es
antonio.luque@ehu.es

Supporting information for this article is available on the WWW under http://www.eurjic.org or from the author.

can be experimentally measured by variable-temperature magnetic susceptibility measurements. The experimental J values reported for this type of dimeric entity present a great dispersion with values ranging from –211 cm^{-1} for $[Cu_2(\mu\text{-Hypox})_4(Cl)_2]Cl_2{\cdot}6H_2O$[14] to –316 cm^{-1} for $\{[Cu_2(\mu\text{-ade})_4(H_2O)_2][Cu(ox)(H_2O)]_2\}_n$[15] (Hypox = 7*H*-hypoxanthine, ox = oxalate anion). Some previous studies, specifically those performed by Sonnenfroh and Kreilick,[16] pointed out the influence of the metal coordination environment on the magnetic properties. Unfortunately, these studies did not take advantage of the quantum chemistry computational resources available today to provide an exhaustive analysis of the structural parameters and chemical factors that play a crucial role in determining the magnitude of the intradimeric magnetic coupling.

In the present work, we studied three new Cu^{II} complexes by using different purine bases as bridging ligands whilst maintaining the same pyramidal CuN_4O chromophore with an axial water molecule in order to carry out some magnetostructural/chemical correlations. In addition, DFT quantum calculations were performed to evaluate the variation in the coupling constant as a function of structural parameters and on the basis of the nature of the bridging ligand.

Results and Discussion

Compounds **1**–**3** contain centrosymmetric $[Cu_2(\mu\text{-pur})_4(H_2O)_2]$ [pur = adeninato (**1**), 7*H*-adenine (**2**) and 6-chloropurinato (**3**)] dimeric entities showing a windmill-shaped arrangement, where two copper(II) atoms are bridged by four purine bases through their N3 and N9 nitrogen atoms establishing a Cu1···Cu1a distance of 2.948–3.001 Å. The copper atoms exhibit a distorted square-pyramidal N_4O_w environment, in which the apical position is occupied by a water molecule. A perspective view of the dimeric entity of compound **2** is given in Figure 1. The labelling scheme used here for the nucleobase is that conventionally accepted for chemical and biological purposes. The structural parameters listed in Table 1 are similar to those reported for dimeric compounds containing μ-κ*N3*:κ*N9* bridging purine ligands.[17]

The purine ligands in compounds **1** and **3** are structurally disordered between two coplanar orientations with inverted coordination modes (μ-κ*N3*:κ*N9*/μ-κ*N9*:κ*N3*, see Scheme 1). This structural disorder could be attributed to several factors: (a) there is just one unique isomer but with different orientations along the crystal structure, (b) the coexistence of more than one isomer or (c) the combination of both.

Similar structural disorder has been found in previous compounds in which the dinuclear entity is built up from the coordination of bridging bicyclic ligands.[3,18] Taking compound **3** as an example, there are four possible isomers compatible with the presence of disorder in all the bridging ligands. The nomenclature used to denominate them is based on the assignment of different terms U (up) or D (down) depending on the coordination of each pyrimidinic N3 atom to the upper or lower metal centre. In this way, the four possible isomers are UUUU, UUUD, UUDD and UDUD (Figure 2). The structure of every isomer was optimized through DFT-based computational calculations to get an estimation of the energy difference among them. The obtained results, for the dimeric entities found in com-

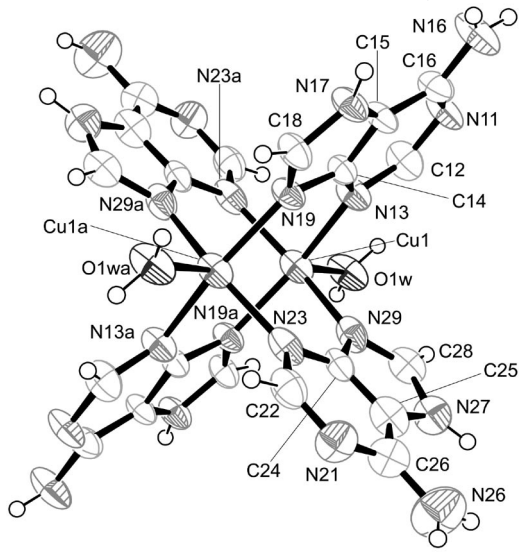

Figure 1. ORTEP view and labelling scheme for the dimeric entity of compound **2** (ellipsoids at 50% probability level).

Table 1. Selected bond lengths [Å] for the coordination polyhedron of compounds **1**–**3**.[a]

Compound **1**			
Cu1–N19	1.991(5)	Cu1–N23a	2.008(6)
Cu1–N29	2.025(5)	Cu1–O1w	2.207(4)
Cu1–N13a	2.020(5)	Cu1···Cu1a	2.948(2)
Compound **2**			
Cu1–N13	1.994(3)	Cu1–N23a	2.000(4)
Cu1–N29	1.970(4)	Cu1–O1w	2.169(2)
Cu1–N19a	2.015(3)	Cu1···Cu1a	3.001(1)
Compound **3**			
Cu1–N19	1.997(4)	Cu1–N29a	2.026(4)
Cu1–N23	2.024(4)	Cu1–O1w	2.124(4)
Cu1–N13a	2.016(4)	Cu1···Cu1a	2.966(2)

[a] Symmetry codes for **1**: a = $-x + 3/2, -y + 1/2, -z + 1$; for **2**: a = $-x + 1, -y, -z + 2$; for **3**: a = $-x + 1/2, -y + 1/2, -z + 1$.

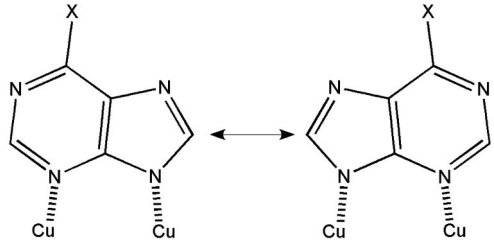

Scheme 1. Coplanar orientations of the disordered purine ligands with different coordination modes.

pounds **1** and **3**, show that the energetic difference is lower than 2 kcal mol^{-1}, a value within the range observed for hydrogen-bonding interactions.[19] These results point out that the supramolecular environment is an important key factor necessary to stabilize a specific isomer of the dimeric entity, and in addition, these results do not preclude the possible presence of a mixture of various isomers in the crystal structures of these compounds.

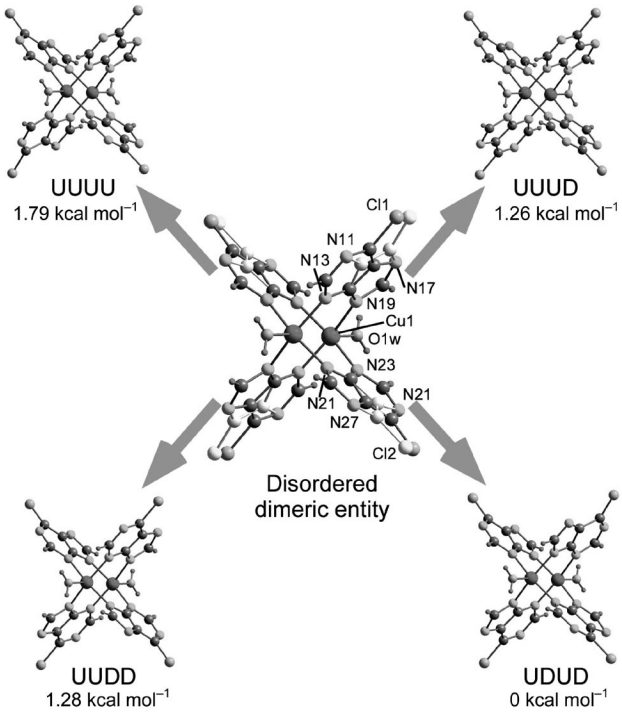

Figure 2. Possible isomers of the disordered dimer in compound **3** and the labelling scheme employed for the crystallographically independent bridging ligands. Relative energy values calculated with the B3LYP/6-31+G(d,p)//B3LYP/6-31G(d) model chemistry.

Crystal Packing of $[Cu_2(\mu\text{-ade})_4(H_2O)_2]\cdot(bpa)\cdot 8H_2O$ (1)

Crystal building of **1** shows an open framework that is essentially maintained by hydrogen-bonding interactions between neutral $[Cu_2(\mu\text{-ade})_4(H_2O)_2]$ entities and in which bpa molecules and water crystallization molecules are inserted (see Supporting Information).

The complex units are linked by two types of hydrogen-bonding interactions, which give rise to an open framework with channels running along the [100] and [001] directions (Figure 3). On the one hand, adeninato ligands belonging to adjacent dimers establish 1D arrays by means of two symmetrical N26–H···N21 hydrogen-bonding interactions. This interaction can involve Watson–Crick or Hoogsteen side, leading to the formation of $R^2_2(8)$ (Watson–Crick/Watson–Crick), $R^2_2(10)$ (Hoogsteen/Hoogsteen) or $R^2_2(9)$ (Watson–Crick/Hoogsteen) hydrogen-bonding rings owing to the mentioned disorder of two adeninato ligands (see Supporting Information). On the other hand, these chains establish additional O1w–H12w···N11 hydrogen-bonding interactions when intercrossed. 1,2-Bis(4-pyridyl)ethane and solvent molecules are placed within the channels. Organic molecules are enclosed by four dimers in such a way that they are inserted in a parallel disposition with respect to the nucleobase rings with an interplanar distance of 3.49 Å, which is indicative of some kind of aromatic stacking (Figure 3a).

Water molecules are disposed along two sorts of channels parallel to the *c* axis (Figure 3b). The smallest channel comprises 115 Å^3 per unit cell and is occupied by the O5w water

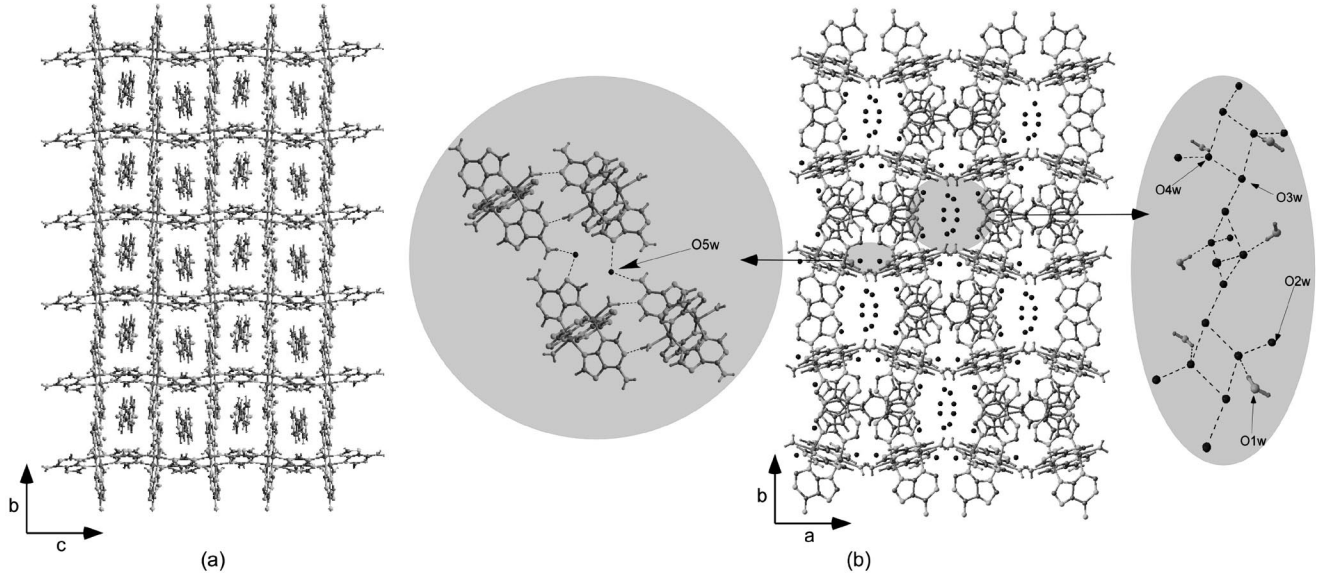

Figure 3. Crystal packing of compound **1**: (a) Insertion of the organic molecules among the dimeric entities; (b) channels where crystallization water molecules are placed.

molecule, which establishes hydrogen bonds with the adeninato ligands. Calculations using PLATON[20] showed that the effective volume for inclusion in the major channel is equal to 971 Å^3 per unit cell (21.6% of the total volume). There, the O3w and O4w water molecules are hydrogen bonded to form [T4(0)A0] 1D tapes.[21] These molecular aggregates are anchored to O2w water molecules, also placed within this channel, to inclusion bpa molecules and to coordinated O1w water molecules.

Supramolecular Architecture of $[Cu_2(\mu\text{-Hade})_4(H_2O)_2]\cdot(NO_3)_4\cdot 2[Cu(pic)_2(H_2O)]\cdot 6H_2O$ (2)

Crystal building of compound **2** contains two different complex units: $[Cu_2(\mu\text{-Hade})_4(H_2O)_2]^{4+}$ dimeric cations and $[Cu(pic)_2(H_2O)]$ neutral monomers, together with crystallization water molecules and nitrate anions, which neutralize the positive charges of the dimeric entities. The copper(II) atom belonging to the monomeric complex shows a square-pyramidal $CuO_2N_2O_w$ environment, in which the basal plane is formed by two chelating picolinato-κ^2N,O ligands with a bite angle of 83.5°, and the copper atom is slightly displaced from the basal plane [0.138 Å] towards the apical position filled by a water molecule (see Supporting Information).

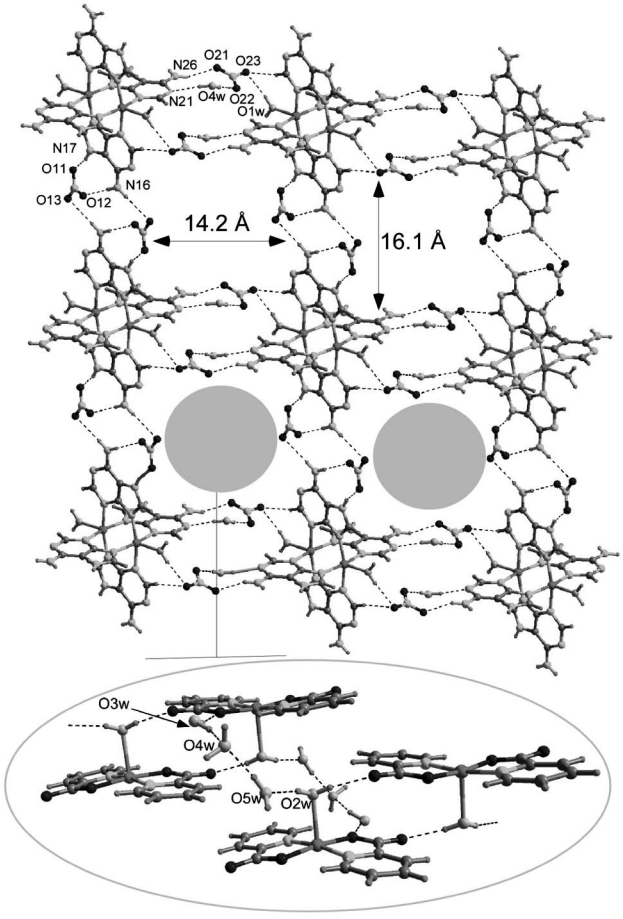

Figure 4. View of the 2D network of compound **2** in which the approximated dimensions of the rectangular channels are specified. Bottom: monomer water chains running along these channels are shown.

The crystal cohesion is maintained both by electrostatic interactions and by an extensive hydrogen-bonding network (Figure 4). The interaction between the Hoogsteen sides of adjacent nucleobases, as it was observed in compound **1**, is precluded because of the protonation in the N7 position of adenine. Therefore the 7*H*-adenine ligands act as hydrogen-bonding donors with nitrate anions as acceptors leading to a $R^2_2(9)$ ring. This interaction is reinforced by the formation of a $R^4_4(12)$ ring connecting both dimeric entities and nitrates giving rise to chains that run along the [110] direction. These chains are further connected by additional hydrogen bonds involving the O4w crystallization water molecule, the nitrate anion, the Watson–Crick face of an adenine ligand and the coordinated O1w water molecule. These interactions lead to a 2D supramolecular network with large holes. The O3w water molecules are placed between these layers to generate a $R^1_2(7)$ hydrogen-bonding pattern with the Hoogsteen face of the adenine ligands, which hold the layers together (see Supporting Information). The large channels of the 3D open framework are occupied by monomeric $[Cu(pic)_2(H_2O)]$ entities and O5w crystallization water molecules. The copper(II) monomers are symmetrically O2w–H22w···O372 hydrogen bonded, which leads to dimeric aggregates that are also anchored to the dimeric complex entities through additional hydrogen bonds. The supramolecular arrangement is reinforced by additional weak π–π contacts between nucleobase rings and the pyridinic ring of the picolinato ligand.

Crystal Packing of $[Cu_2(\mu\text{-6Clpur})_4(H_2O)_2]\cdot\sim 6H_2O$ (3)

Its structure is made up of neutral $[Cu_2(\mu\text{-6Clpur})_4(H_2O)_2]$ dimers and crystallization water molecules that take part in an extensive network of hydrogen bonds. The 6-chloropurinato ligand shows the same coordination mode observed for the adenine complexes. As far as we are aware, there is only one other example in the CSD database[22] of a 7*H*-6-chloropurine molecule coordinated to a metal, the [Co(6-chloropurine)(dimethylglyoximato)$_2$(methyl)] complex.[23] In contrast to what happens in compound **3**, the ligand remains neutral and it is coordinated to the metal centre through the pyrimidinic N3 position.

As a consequence of the lack of heteroatomic hydrogen atoms in the bridging ligand, the hydrogen-bonding interactions among the dimeric entities take place through crystallization water molecules, as it has been mentioned for compound **2**. It is worth to note that the distance between the exocyclic Cl2 atoms from two adjacent complex units is only 3.3 Å (Figure 5). Some research groups have studied these interactions as a result of the controversy that exists about them, concluding that in chlorine atoms the van der Waals radii describe an elliptic distribution and not a spherical one. This fact produces lower repulsion, and thus, closer Cl···Cl contacts in certain directions could be

observed.[24] The observed Cl···Cl distance is comparable to those found in previously reported compounds in which a chlorine atom is bonded to the C6 atom of the purine base.[25] In contrast, the Cl1 atoms are perpendicularly oriented towards the purine ring of an adjacent dimer, pointing out the nitrogen N21 atom with a distance of 3.2 Å. Previous theoretical work performed on a series of azaaromatic chloride compounds established that this type of Cl···N contact is weakly attractive. In order to analyze this interaction in more detail, the electrostatic potential surface of the dimeric entity was calculated (Figure 6). It can be observed that the chlorine atom presents a positive potential area at its top, so in its perpendicular orientation towards the purine ring, the chlorine atom is attracted by the N21 atom, which has a potential with the opposite sign.

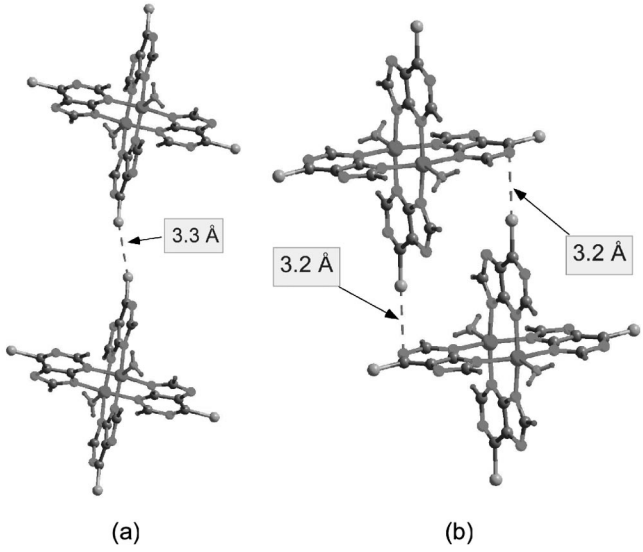

Figure 5. (a) Interdimeric Cl···Cl contact and (b) T-shaped noncovalent Cl···N interaction.

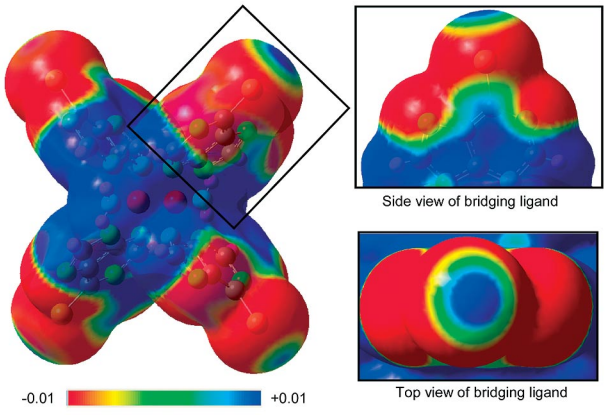

Figure 6. Electrostatic potential performed upon an electronic isodensity surface of 0.001 a.u. for the dimeric $[Cu_2(\mu\text{-}6Clpur)_4(H_2O)_2]$ entity.

In addition to these unusual interactions involving the chlorine atoms of the purine ligand, additional hydrogen-bonding interactions are also present. The 3D arrangement of the complex entities generates channels parallel to the *b* axis that are occupied by water crystallization molecules (Figure 7).

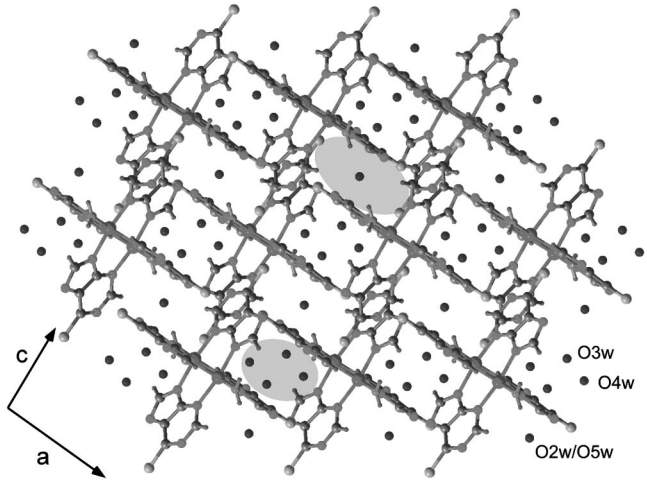

Figure 7. View of the packing of compound **3** along the *ac* plane showing the channels occupied by the crystallization water molecules.

Magnetic Properties

The thermal evolution of the molar magnetic susceptibility (χ_M) and the $\chi_M T$ product for compounds **1** and **3** are quite similar, and they are indicative of strong intradimeric antiferromagnetic interactions (see Supporting Information). The χ_M curve suffers an initial rise upon cooling from room temperature to gain the maximum value at 180 and 220 K, respectively. Afterwards, it decreases and reaches a minimum value in the vicinity of 50 K and increases again at lower temperatures as a result of the presence of paramagnetic impurities. In compound **2** the expected maximum in the susceptibility curve is not observed due to the coexistence within the crystal structure of the paramagnetic monomers. In all cases, the room-temperature $\chi_M T$ values are lower than that expected for an uncoupled paramagnetic $S = 1/2$ centre (0.375 $cm^3 mol^{-1} K$, $g = 2.0$). Continuous drop is observed to reach a plateau below 50 K for compounds **1** and **3**, attributed to the presence of a small amount of paramagnetic impurities. In compound **2** this plateau is reached at 65 K and takes a value of 0.216 $cm^3 mol^{-1} K$. This value is retained up to 10 K, after which a very slight lowering is observed in good agreement with the presence of an almost uncoupled monomeric copper atom per each dimeric copper atom.

The experimental magnetic data were fitted by using the Bleaney–Bowers equation ($H = -JS_1S_2$) for a dinuclear copper(II) complex[26] modified to take into account the presence of the paramagnetic impurities for compounds **1** and **3**. In compound **2**, an additional term accounting for the

presence of uncoupled monomeric Cu^{II} entities was included. The best-fit values are reported in Table 2. The obtained *J* values fall within the range previously reported for compounds with $[Cu_2(\mu\text{-pur})_4(X)_2]^{n+}$ (n = 0, 2, 4; X = H_2O, Cl, Br) entities,[3–7,16–18,27] which range from –211 to –316 cm^{-1} (Table 3). The dispersion of the *J* values, ca. 105 cm^{-1}, indicates that structural/chemical parameters strongly influence the magnitude of the magnetic coupling.

Table 2. Experimental values for the magnetic fit of compounds **1**–**3**.

Compound	$\chi_M T$[a]	T_{max}[b]	J_{exp}[c]	ρ[d]	g
1	0.312	180	–222	7.9	2.13
2	0.326	—	–288	50.0	2.15
3	0.233	220	–250	1.1	2.15

[a] Room-temperature value [$cm^3 mol^{-1} K$]. [b] Temperature of the maximum value [K]. [c] Experimental value of the magnetic coupling constant [cm^{-1}]. [d] Paramagnetic impurity percentage.

In order to analyze the magnetic behaviour of these compounds, DFTUB3LYP calculations were carried out. The correlation between the *J* value and some structural parameters was evaluated upon models based on the crystallographic data of the $[Cu_2(\mu\text{-ade})_4(H_2O)_2]$ entity of compound **1**. In compounds with short $Cu^{II}\cdots Cu^{II}$ distances (less than 3.10 Å), the magnetic interaction may result from direct interaction of the d orbitals of the metal atom (exchange pathway) or may involve molecular orbitals of the bridging ligands (superexchange pathway). The calculated *J* value (+17 cm^{-1}) for a model in which the adeninato ligands have been replaced by terminal ammonia groups seems to point to the superexchange pathway being responsible for the antiferromagnetic behaviour of these compounds. Thus, magnetic orbitals must be built from the interaction between $d_{x^2-y^2}$ atomic orbitals of metal centres and those of purine ligands that have an appropriate symmetry to interact with them. Figure 8 shows the SOMO orbitals of the $[Cu_2(\mu\text{-ade})_4(H_2O)_2]$ entity in the triplet state. The presence or absence of a nodal plane on the C4 atom is responsible for the energy difference between the two SOMO orbitals and, as a consequence, of the magnitude of the antiferromagnetic behaviour of the compounds.

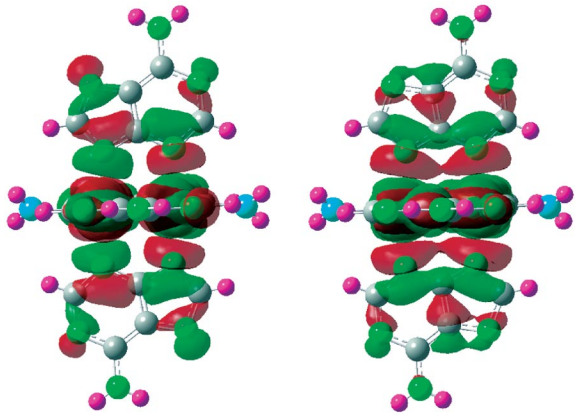

Figure 8. Representation of SOMO orbitals for the triplet state (S = 1) upon the $[Cu_2(\mu\text{-ade})_4(H_2O)_2]$ entity of compound **1**.

With the aim of evaluating the influence of the variations in the structural features upon the magnetic behaviour, three main structural parameters were considered: copper–nitrogen, copper–water molecule and copper···copper distances (Figure 9). The decrease in the Cu–N distances favours the interaction between the magnetic orbitals of the metal and the ligands and reinforces the antiferromagnetism. On the contrary, a shorter Cu–Ow distance brings a decrease in the antiferromagnetism as a result of the increase in the d_{z^2} character of the magnetic orbitals (decreasing the $d_{x^2-y^2}$ character), as previously reported by Sonnenfroh and Kreilick.[16] In contrast, longer metal···metal distances cause an increase in the antiferromagnetic interactions.

To explain this latter behaviour, it is necessary to pay attention to the orbitals of the bridging ligand, whose lobes positioned on the N3 and N9 atoms become hybridized as the copper···copper distance increases. As a result, a greater overlapping of the lobes is generated in the vicinity of the C4 atom, increasing the energy difference between the resulting magnetic orbitals (Scheme 2).

As the effect of these structural parameters on the magnetic coupling is of the same order of magnitude, any attempt to obtain experimental magnetostructural corre-

Table 3. Structural parameters and *J* values of some representative compounds together with those observed for compounds **1**–**3**.

Compound formula	Cu–N[a]	Cu–X[b]	Cu···Cu[c]	T_{max}	J_{exp}	Ref.
$[Cu_2(\mu\text{-ade})_4(NH_3)_2]\cdot 6H_2O$	–	–	–	222	–	[16]
$[Cu_2(\mu\text{-ade})_4(H_2O)_2]\cdot(bpa)\cdot 8H_2O$	2.01	2.21	2.95	180	–222	this work
$[Cu_2(\mu\text{-ade})_4(Pip)_2]\cdot 6H_2O$	–	–	–	210	–246	[16]
$[Cu_2(\mu\text{-ade})_4(H_2O)_2]\cdot 5H_2O$	2.02	2.20	2.95	–	–257	[3]
$\{[Cu_2(\mu\text{-ade})_4(H_2O)_2][Cu(oda)(H_2O)]_4\}$	2.01	2.18	2.94	–	–274	[27]
$\{[Cu_2(\mu\text{-ade})_4(H_2O)_2][Cu(ox)(H_2O)]_2\}_n$	2.01	2.17	2.94	–	–316	[15]
$[Cu_2(\mu\text{-Hade})_4Br_2]Br_2\cdot 2H_2O$	–	–	–	–	–284	[4]
$[Cu_2(\mu\text{-Hade})_4(H_2O)_2](NO_3)_4\cdot 2[Cu(pic)_2(H_2O)]\cdot 6H_2O$	2.00	2.17	3.00	–	–288	this work
$[Cu_2(\mu\text{-Hade})_4Cl_2]Cl_2\cdot 6H_2O$	2.03	2.43	3.07	251	–285	[6]
$[Cu_2(\mu\text{-Hade})_4(H_2O)_2](SO_4)\cdot 6H_2O$	–	–	–	253	–305	[16]
$[Cu_2(\mu\text{-Hade})_4(H_2O)_2](ClO_4)\cdot 2H_2O$	2.03	2.17	2.95	243	–312	[5,16]
$[Cu_2(\mu\text{-hypox})_4Cl_2]Cl_2\cdot 6H_2O$	2.00	2.43	3.02	212	–211	[14,16]
$[Cu_2(\mu\text{-hypox})_4Br_2]Br_2\cdot 2H_2O$	–	–	–	–	–284	[4]
$[Cu_2(\mu\text{-6Clpur})_4(H_2O)_2]\cdot\sim 6H_2O$	2.02	2.12	2.97	220	–250	this work

[a] Equatorial cooper–nitrogen distance. [b] Axial copper–ligand distance. [c] Distance between intradimeric copper atoms.

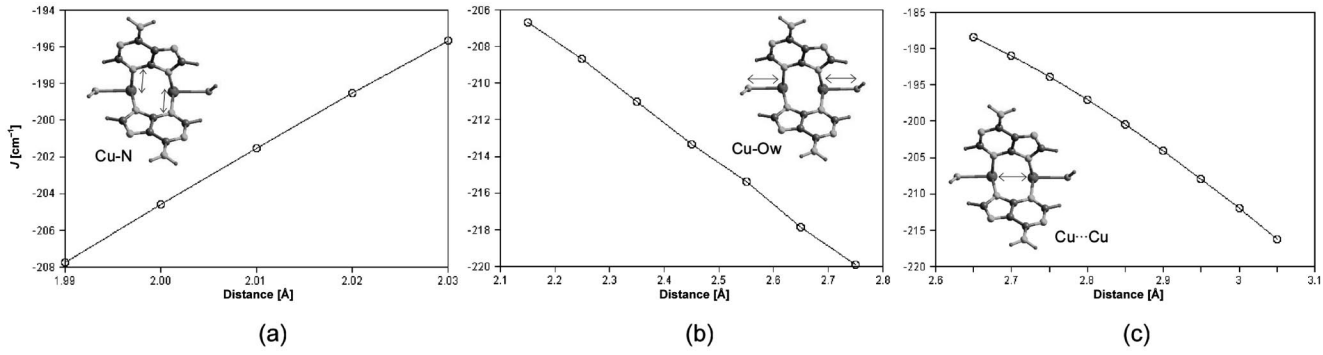

Figure 9. Variation in the magnetic coupling constant value as a function of (a) the Cu–N bond equatorial distances, (b) the Cu–Ow bond axial distance and (c) the Cu···Cu distance.

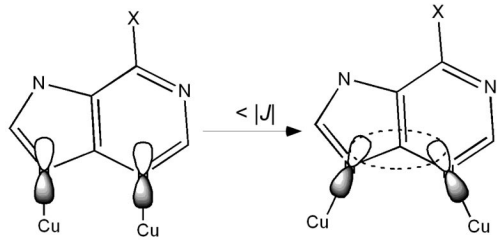

Scheme 2. Increase in the magnetic coupling constant as a result of a greater overlap around the middle carbon atom.

lations on the basis of just one parameter is precluded. With the aim of verifying if the simultaneous effect of all these structural factors can reproduce the wide range of experimentally reported *J* values, the structural parameters of the adenine-bridged dimeric entity were modified to obtain a maximum and a minimum value of the antiferromagnetic coupling constant. The calculated *J* values, –289 and –181 cm^{-1}, give a difference of 108 cm^{-1}, which is similar to the experimentally observed range.

It is interesting to note that the charge of the bridging ligand and its substituents may also play an important role in the magnitude of the antiferromagnetic interaction. The *J* value for different models maintaining the same structural parameters but modifying the bridging ligand by adding different substituents in the C6-position was calculated. The calculated *J* values show the relative order: 7*H*-adenine (–267 cm^{-1}) > 7*H*-hypoxanthine (–243 cm^{-1}) > 6-chloro-7*H*-purine (–242 cm^{-1}) > adeninato (–199 cm^{-1}) > hypoxanthinato (–181 cm^{-1}) > 6-chloropurinato (–174 cm^{-1}) (Scheme 3).

This order can be related to the increase in the number of electron lone pairs in the bridging ligand (by means of the deprotonation or by substitution of the exocyclic amine group by a chlorine atom). This fact increases the extension of the molecular orbitals of the bridging ligands and the N3 and N9 atoms contribute to a lesser extent, so they overlap less efficiently with the metal-centred magnetic orbitals and a weaker antiferromagnetic interaction is observed.

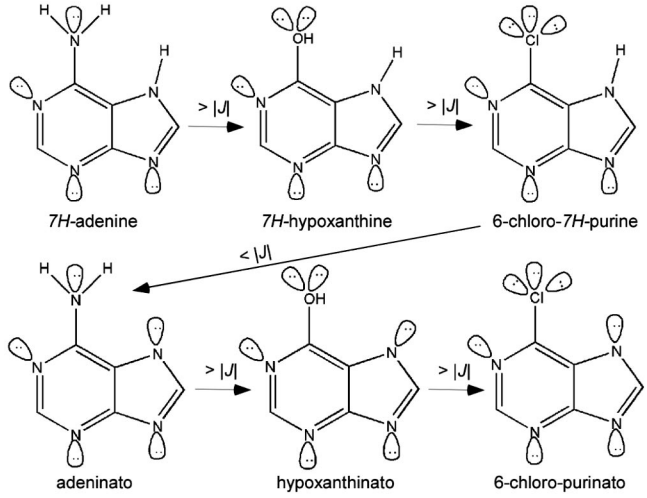

Scheme 3. Calculated order of the bridging ligands according to their ability to transmit magnetic interactions by the superexchange pathway.

Conclusions

It has been proved that $[Cu_2(\mu\text{-purine derivative})_4(H_2O)_2]^{n+}$ entities are robust enough to allow chemical modifications, such as deprotonation or substituent modifications, without remarkable changes in its windmill dimeric structure. In addition, its great versatility as supramolecular synthon permits the inclusion of organic molecules and even of complex entities. In contrast, the magnitude of the antiferromagnetic coupling in these compounds is governed by both structural and chemical parameters. The shortening of the copper–nitrogen distance and the elongation of the copper–Ow and Cu···Cu distances strengthen the antiferromagnetic coupling. Modifications of the bridging ligands that involve an increase in the number of electron lone pairs lead to a weakening of the antiferromagnetic interactions.

Experimental Section

Reagents: All chemicals were of reagent grade and used as commercially obtained.

Physical Measurements: Elemental analyses (C, H, N) were performed with a Perkin–Elmer Analyst 100 microanalytical analyser. Metal content was determined by absorption spectrometry. The IR spectra (KBr pellets) were recorded with an FTIR 8400S Shimadzu spectrometer in the 4000–400 cm^{-1} spectral region. Magnetic measurements were performed on polycrystalline samples of the complexes taken from the same uniform batches used for the structural determinations with a Quantum Design SQUID susceptometer covering the temperature range 5.0–300 K at a magnetic field of 1000 G. The susceptibility data were corrected for the diamagnetism estimated from Pascal's Tables,[28] the temperature-independent paramagnetism and the magnetization of the sample holder. Thermal analyses (TG/DTA) were performed with a TA Instruments SDT 2960 thermal analyser in a synthetic air atmosphere (79% N_2/21% O_2) with a heating rate of 5 °C min^{-1}.

X-ray Structural Studies: Diffraction data were collected at 293(2) K with Oxford Diffraction Xcalibur (for **1** and **2**) and at 150(2) K with STOE IPDS (for **3**) diffractometers with graphite-monochromated Mo-K_α radiation (λ = 0.71073 Å). The data reduction was done with the CrysAlis RED[29] and X-RED[30] programs. Structures were solved by direct methods by using the SIR92 program[31] and refined by full-matrix least-squares on F^2 including all reflections (SHELXL97).[32] All calculations were performed by using the WINGX crystallographic software package.[33] In compound **3**, the O5w crystallization water molecule was refined with a partial occupation factor in agreement with the performed thermogravimetric measurements. Crystal parameters and details of the final refinements of compounds **1**–**3** are summarized in Table 4. CCDC-796960 (for **1**), -796961 (for **2**) and -796962 (for **3**) contain the supplementary crystallographic data for this paper. These data can be obtained free of charge from The Cambridge Crystallographic Data Centre via www.ccdc.cam.ac.uk/data_request/cif.

Computational Details: Energy quantum mechanical calculations for all the isomers of dimeric entities of compounds **1**–**3** were carried out by using two different model chemistries, B3LYP/6-311+G(d,p)//B3LYP/6-31G(d) and B3PW91/6-311+G(d,p)//B3LYP/6-31G(d), in order to ensure the validity of the results (see the Supporting Information).[34] A detailed description of the computational strategy adopted in this work to compute the magnetic coupling constant ($J_{calcd.}$) values was described elsewhere.[35] Density functional theory, B3LYP/6-31G(d), was used to carry out two separate calculations to evaluate the coupling constant of each compound. One calculation was used to determine the high-spin state and the other one to determine the low-spin broken symmetry state. The correctness of the latter state was ensured by its spin density distribution. The Gaussian 03 program[36] was employed throughout this work.

$[Cu_2(\mu\text{-ade})_4(H_2O)_2]\cdot(bpa)\cdot 8H_2O$ (1): An aqueous methanol solution (1:1, 8 mL) of the bpa ligand (0.0186g, 0.1 mmol) was added to another aqueous methanol solution (25 mL) containing $Cu(NO_3)_2\cdot 3H_2O$ (0.0488 g, 0.2 mmol) and adenine (0.0546 g, 0.4 mmol) with continuous stirring at 50 °C. The resulting solution was neutralized with the addition of KOH to pH 9.0. Deep-blue-coloured single crystals were obtained after 1 d. Yield: 80% (based on metal). $C_{16}H_{24}CuN_{11}O_5$ (514.00): calcd. C 37.35, H 4.67, N 29.96, Cu 12.36; found C 37.39, H 4.72, N 29.97, Cu 12.36. IR (KBr pellet): $\tilde{\nu}$ = 3435 [s, ν(O–H)]; 3195 [s, $\nu(NH_2)$]; 3105 [sh., ν(C–H)]; 1605 (s), 1560 [m, ν(C=C) + $\delta(NH_2)$]; 1460 [m, δ(C–H) + ν(C=C + C=N)]; 1380 (m, δ_{ring}); 1340 [w, δ(C2–H2) + δ(C4–C5)]; 1300 [w, δ(C2–H2) + ν_{ring}]; 1271 [w, δ(C–H) + ν(N7–C8)]; 1150 [m, ν(C8–N9)]; 1025 (w, δ_{ring}); 1005 [m, $\tau(NH_2)$]; 940 [w, δ(C8)]; 735 (w), 655 (m, δ_{ring}); 535 [m, (Cu–N3)] cm^{-1}.

$[Cu_2(\mu\text{-Hade})_4(H_2O)_2](NO_3)_4\cdot 2[Cu(pic)_2(H_2O)]\cdot 6H_2O$ (2): An aqueous methanol solution (1:1, 35 mL) containing adenine (0.1365 g, 1 mmol) and 2-pyridinecarboxaldehyde (95.1 µL, 1 mmol) was kept under reflux for 2 h, and this mixture was then treated with $Cu(NO_3)_2\cdot 3H_2O$ (0.2440 g, 1 mmol) dissolved in methanol (10 mL). Five weeks later, a few dark-blue single crystals of **2** appeared in the solution. Yield: 15% (based on metal).

Table 4. Single-crystal data and structure refinement details for compounds **1**–**3**.

	1	**2**	**3**
Formula	$C_{16}H_{24}CuN_{11}O_5$	$C_{22}H_{28}Cu_2N_{14}O_{15}$	$C_{10}H_6Cl_2CuN_8O\cdot\sim 3H_2O$
Weight [g mol^{-1}]	514.00	855.64	442.70
Crystal system	monoclinic	triclinic	monoclinic
Space group	*C*2/*c*	$P\bar{1}$	*C*2/*c*
a [Å]	16.534(1)	9.746(1)	16.060(2)
b [Å]	19.646(1)	12.971(2)	13.502(1)
c [Å]	14.181(1)	13.699(2)	15.955(2)
α [°]	90	92.28(1)	90
β [°]	102.092(7)	107.97(1)	112.49(1)
γ [°]	90	90.60(1)	90
V [$Å^3$]	4504.2(5)	1645.6(4)	3196.7(6)
Z	8	2	8
$\rho_{calcd.}$ [g cm^{-3}]	1.516	1.727	1.840
$\rho_{obsd.}$ [g cm^{-3}]	1.52(2)	1.73(3)	1.84(1)
μ [mm^{-1}]	1.023	1.385	1.738
Temperature [K]	293(2)	293(2)	150(2)
Reflections collected	12239	12146	9816
Unique data/parameters	3976/284	7988/478	3138/241
R_{int}	0.0684	0.0503	0.0608
Reflections with $I \geq 2\sigma(I)$	1137	2487	1337
Goodness of fit (*S*)[a]	0.973	0.982	0.971
R_1[b]/wR_2[c] [$I \geq 2\sigma(I)$]	0.0539/0.1304	0.0468/0.0884	0.0356/0.0550
R_1/wR_2 [all data]	0.0912/0.1486	0.1046/0.0974	0.0980/0.0628

[a] $S = [\sum w(F_o^2 - F_c^2)^2/(N_{obsd.} - N_{param.})]^{1/2}$. [b] $R_1 = \sum||F_o|-|F_c||/\sum|F_o|$. [c] $wR_2 = [\sum w(F_o^2 - F_c^2)^2/\sum w|F_o|^2]^{1/2}$; $w = 1/[\sigma^2(F_o^2) + (aP)^2]$, where $P = [\max(F_o^2,0) + 2F_c^2]/3$ with a = 0.0756 (for **1**), 0.0436 (for **2**) and 0.0225 (for **3**).

$C_{22}H_{28}Cu_2N_{14}O_{15}$ (855.64): calcd. C 30.88, H 3.29, N 22.92, Cu 14.85; found C 30.90, H 3.27, N 22.91, Cu 14.88. IR (KBr pellet): $\tilde{\nu}$ = 3390 [s, ν(O–H)]; 3208 (s, $\nu(NH_2)$]; 3125 [sh., ν(C–H)]; 1670 [s, ν_{as}(O–C–O)]; 1603 (s), 1572 [sh., ν(C=C) + $\delta(NH_2)$]; 1475 [m, δ(C–H) + ν(C=C + C=N)]; 1383 [s, $\nu(NO_3)$]; 1405 (sh., δ_{ring}); 1356 [sh., δ(C2–H2) + δ(C4–C5)]; 1315 [m, δ(C2–H2) + ν_{ring}]; 1260 [w, δ(C–H) + ν(N7–C8)]; 1148 [w, ν(C8–N9)]; 1028 (sh.; ring deformation); 938 [w, δ(C8)]; 738 (w), 656 (w, δ_{ring}); 551 (w), 456 [w, (Cu–N3)] cm^{-1}.

$[Cu_2(\mu\text{-}6Clpur)_4(H_2O)_2]\cdot\sim 6H_2O$ (3): Purple crystals of compound **3** were prepared by slow diffusion of an aqueous methanol solution (1:1) of 6-chloropurine (0.0624 g, 0.2 mmol) into an aqueous solution of $Cu(NO_3)_2\cdot 3H_2O$ (0.0247 g, 0.1 mmol). Crystal growth was observed 3 weeks later. Yield: 40% (based on metal). $C_{10}H_6Cl_2CuN_8O\cdot\sim 3H_2O$ (442.7): calcd. C 27.13, H 2.73, N 25.31, Cu 14.35; found C 27.12, H 2.69, N 25.28, Cu 14.37. IR (KBr pellet): $\tilde{\nu}$ = 3410 [s, ν(O–H)]; 3115 [sh., ν(C–H)]; 1620 [sh., ν(C5=C6 + C2=N3)]; 1598 (s), 1589 [sh., ν(C=C) + $\delta(NH_2)$]; 1465 [w, δ(C–H) + ν(C=C + C=N)]; 1400 (w, ring deformation); 1328 [m, δ(C2–H2) + δ(C4–C5)]; 1259 [w, δ(C–H) + ν(N7–C8)]; 1184 [m, ν(C8–N9)]; 1026 (w, δ_{ring}); 953 [w, δ(C8)]; 637 (w, δ_{ring}); 545 [w, (Cu–N3)] cm^{-1}.

Supporting Information (see footnote on the first page of this article): Structural parameters of hydrogen-bonding interactions of compounds **1**–**3**; computationally obtained energy values for isomers of the dimeric entities of compounds **1**–**3**; TGA/DTA curve and analysis of **2**; magnetic data for compounds **1**–**3**; ORTEP views of the dimeric entities of compounds **1**–**3**; additional figures for compounds **1** and **2**.

Acknowledgments

This work was supported by the Ministerio de Ciencia e Innovación (MAT2008–05690/MAT) and the Gobierno Vasco (IT-280–07). S. P.-Y. and J. C. thank Universidad del País Vasco/Euskal Herriko Unibertsitatea for a predoctoral fellowship (PIFA01/2007/021). The SGI/IZO-SGIker UPV/EHU, financed by the National Program for the Promotion of Human Resources within the National Plan of Scientific Research, Development and Innovation "Ministerio de Ciencia e Innovación", "Fondo Social Europeo (FSE)" and "Gobierno Vasco/Eusko Jaurlaritza, Dirección de Política Científica" is gratefully acknowledged for generous allocations.

[1] a) E. Bouwman, W. L. Driessen, J. Reedijk, *Coord. Chem. Rev.* **1990**, *104*, 143–172; b) P. O'Brien, *Coord. Chem. Rev.* **1984**, *58*, 169–244; c) O. Khan in *Molecular Magnetism*, VCH, New York, **1993**.
[2] a) D. J. Hodgson, *Prog. Inorg. Chem.* **1975**, *19*, 173–241; b) M. Melnik, *Coord. Chem. Rev.* **1982**, *42*, 259–293.
[3] E. Sletten, *Acta Crystallogr., Sect. B* **1969**, *25*, 1480–1491.
[4] T. Asakawa, M. Innoue, K.-I. Hara, M. Kubo, *Bull. Chem. Soc. Jpn.* **1972**, *45*, 1054–1057.
[5] A. Terzis, A. L. Beauchamp, R. Rivest, *Inorg. Chem.* **1973**, *12*, 1166–1170.
[6] P. De Meester, A. C. Skapski, *J. Chem. Soc.* **1971**, *A13*, 2167–2169.
[7] E. Sletten, *Chem. Commun. (London)* **1967**, 1119–1120.
[8] a) P. J. Sanz Miguel, B. Lippert, *Dalton Trans.* **2005**, 1679–1686; b) A. M. Beatty, *Coord. Chem. Rev.* **2003**, *246*, 131–143.
[9] a) J.-M. Lehn, *Angew. Chem. Int. Ed. Engl.* **1990**, *29*, 1304–1319; b) G. R. Desiraju in *Crystal Engineering: The Design of Organic Solids*, Elsevier, Amsterdam, **1989**.
[10] A. D. Burrows, C.-W. Chan, M. M. Chowdry, J. E. McGrady, D. M. P. Mingos, *Chem. Soc. Rev.* **1995**, *24*, 329–339.
[11] D. J. Cram, J. M. Cram in *Container Molecules and Their Guests*, Royal Society of Chemistry Monographs in Supramolecular Chemistry (Ed.: J. F. Stoddart), Royal Society of Chemistry, Cambridge, **1994**.
[12] D. Choquesillo-Lazarte, M. D. Brandi-Blanco, I. García-Santos, J. M. González-Pérez, A. Castiñeiras, J. Niclós-Gutiérrez, *Coord. Chem. Rev.* **2008**, *252*, 1241–1256.
[13] J. Casanova, G. Alzuet, J. Latorre, J. Borras, *Inorg. Chem.* **1997**, *36*, 2052–2058.
[14] E. Sletten, *Acta Crystallogr., Sect. B* **1970**, *26*, 1609–1614.
[15] J. P. García-Terán, O. Castillo, A. Luque, U. García-Couceiro, P. Román, L. Lezama, *Inorg. Chem.* **2004**, *43*, 4549.
[16] D. Sonnenfroh, R. W. Kreilick, *Inorg. Chem.* **1980**, *19*, 1259–1262.
[17] a) J. W. Suggs, M. J. Dube, M. Nichols, *J. Chem. Soc., Chem. Commun.* **1993**, 307–309; b) C. H. Wei, K. B. Jacobson, *Inorg. Chem.* **1981**, *20*, 356–363; c) . C. Gagnon, J. Hubert, R. Rivest, A. L. Beauchamp, *Inorg. Chem.* **1977**, *16*, 2469–2473.
[18] a) E. J. Gao, Q. T. Liu, *Acta Chim. Sinica* **2005**, *63*, 725–728; b) M. Tayebani, K. Feghali, S. Gambarotta, G. P. A. Yap, *Inorg. Chem.* **2001**, *40*, 1399–1401; c) F. C. Zhu, H. W. Schmalle, E. Dubler, *Acta Crystallogr., Sect. C* **1998**, *54*, 733–737; d) E. Sletten, *Acta Crystallogr., Sect. B* **1970**, *26*, 1609–1614.
[19] T. H. Dunning Jr, *J. Phys. Chem. A* **2000**, *104*, 9062–9080.
[20] A. L. Spek, *PLATON*, Utrecht University, Utrecht, Holland **1998**.
[21] L. Infantes, S. Motherwell, *Cryst. Eng. Commun.* **2002**, *4*, 454–461.
[22] F. H. Allen, *Acta Crystallogr., Sect. B* **2002**, *58*, 380–388.
[23] C. Dalby, C. Bleasdale, W. Clegg, M. R. J. Elsegood, B. T. Golding, R. J. Griffin, *Angew. Chem. Int. Ed. Engl.* **1993**, *32*, 1696–1697.
[24] S. L. Price, A. J. Stone, J. Lucas, R. S. Rowland, A. E. Thornley, *J. Am. Chem. Soc.* **1994**, *116*, 4910–4918.
[25] W. Lu, S. Sengupta, J. L. Petersen, N. G. Akhmedov, X. D. Shi, *J. Org. Chem.* **2007**, *72*, 5012–5015.
[26] B. Bleaney, K. D. Bowers, *Proc. Roy. Soc. Ser. A* **1952**, *214*, 451–465.
[27] J. M. González-Pérez, C. Alarcón-Payer, A. Castiñeiras, T. Pivetta, L. Lezama, D. Choquesillo-Lazarte, G. Crisponi, J. Niclós-Gutiérrez, *Inorg. Chem.* **2006**, *45*, 877.
[28] A. Earnshaw, *Introduction to Magnetochemistry*, Academic Press, London, **1968**.
[29] *CrysAlis RED*, version 1.170, Oxford Diffraction, Wroclaw, Poland, **2003**.
[30] *STADI4* and *X-RED*, Stoe & Cie GmbH, Darmstadt, Germany, **2002**.
[31] A. Altomare, M. Cascarano, C. Giacovazzo, A. Guagliardi, *J. Appl. Crystallogr.* **1993**, *26*, 343–350.
[32] G. M. Sheldrick, *SHELXL97*, University of Göttingen, Göttingen, Germany, **1997**.
[33] L. J. Farrugia, *WINGX: A Windows Program for Crystal Structure Analysis*, University of Glasgow, Glasgow, Great Britain, **1998**.
[34] a) A. D. Becke, *Phys. Rev. A* **1998**, *38*, 3098–3100; b) A. D. Becke, *J. Chem. Phys.* **1993**, *98*, 5648–5652; c) C. Lee, W. Yang, R. G. Parr, *Phys. Rev. B* **1988**, *37*, 785–789; d) B. Miehlich, A. Savin, H. Stoll, H. Preuss, *Phys. Lett.* **1989**, *157*, 200–206.
[35] a) E. Ruiz, J. Cano, S. Álvarez, P. Alemany, *J. Comput. Chem.* **1999**, *20*, 1391–1400; b) E. Ruiz, P. Alemany, S. Álvarez, J. Cano, *J. Am. Chem. Soc.* **1997**, *119*, 1297–1303; c) E. Ruiz, A. Rodriguez-Fortea, J. Cano, S. Álvarez, P. Alemany, *J. Comput. Chem.* **2003**, *24*, 982–989; d) E. Rudberg, P. Salek, Z. Rinkevicius, H. Agren, *J. Chem. Theory Comput.* **2006**, *2*, 981–989.
[36] M. J. Frisch, G. W. Trucks, H. B. Schlegel, G. E. Scuseria, M. A. Robb, J. R. Cheeseman, J. A. Montgomery Jr, T. Vreven, K. N. Kudin, J. C. Burant, J. M. Millam, S. S. Iyengar, J. Tomasi, V. Barone, B. Mennucci, M. Cossi, G. Scalmani, N. Rega, G. A. Petersson, H. Nakatsuji, M. Hada, M. Ehara, K. Toyota, R. Fukuda, J. Hasegawa, M. Ishida, T. Nakajima, Y. Honda,

O. Kitao, H. Nakai, M. Klene, X. Li, J. E. Knox, H. P. Hratchian, J. B. Cross, V. Bakken, C. Adamo, J. Jaramillo, R. Gomperts, R. E. Stratmann, O. Yazyev, A. J. Austin, R. Cammi, C. Pomelli, J. W. Ochterski, P. Y. Ayala, K. Morokuma, G. A. Voth, P. Salvador, J. J. Dannenberg, V. G. Zakrzewski, S. Dapprich, A. D. Daniels, M. C. Strain, O. Farkas, D. K. Malick, A. D. Rabuck, K. Raghavachari, J. B. Foresman, J. V. Ortiz, Q. Cui, A. G. Baboul, S. Clifford, J. Cioslowski, B. B. Stefanov, G. Liu, A. Liashenko, P. Piskorz, I. Komaromi, R. L. Martin, D. J. Fox, T. Keith, M. A. Al-Laham, C. Y. Peng, A. Nanayakkara, M. Challacombe, P. M. W. Gill, B. Johnson, W. Chen, M. W. Wong, C. González, J. A. Pople, *Gaussian 03*, revision C.02, Gaussian, Inc., Wallingford, CT, **2004**.

Received: January 23, 2009
Published Online: April 23, 2009

